2-8-2011

Decreased stability and increased formation of soluble aggregates by immature superoxide dismutase do not account for disease severity in ALS.

Kenrick A Vassall

Helen R Stubbs

Heather A Primmer

Ming Sze Tong

Sarah M Sullivan

See next page for additional authors

Citation of this paper:
PMID: 21257910

Authors
Kenrick A Vassall, Helen R Stubbs, Heather A Primmer, Ming Sze Tong, Sarah M Sullivan, Ryan Sobering, Saipraveen Srinivasan, Lee-Ann K Briere, Stanley D Dunn, Wilfredo Colón, and Elizabeth M Meiering

Decreased stability and increased formation of soluble aggregates by immature superoxide dismutase do not account for disease severity in ALS

Kenrick A. Vassall[a,1], Helen R. Stubbs[a,1], Heather A. Primmer[a], Ming Sze Tong[a], Sarah M. Sullivan[a], Ryan Sobering[a,2], Saipraveen Srinivasan[b], Lee-Ann K. Briere[c], Stanley D. Dunn[c], Wilfredo Colón[b], and Elizabeth M. Meiering[a,3]

[a]Guelph-Waterloo Centre for Graduate Studies in Chemistry and Biochemistry and Department of Chemistry, Waterloo, ON, Canada N2L 3G1; [c]Department of Biochemistry, University of Western Ontario, London, ON, Canada N6A 5C1; and [b]Department of Chemistry and Chemical Biology, Rensselaer Polytechnic Institute, 110 8th Street, Troy, NY 12180

Edited by Alan R. Fersht, Media Research Council Laboratory of Molecular Biology, Cambridge, United Kingdom, and approved December 6, 2010 (received for review November 11, 2009)

Protein aggregation is a hallmark of many diseases, including amyotrophic lateral sclerosis (ALS), where aggregation of Cu/Zn superoxide dismutase (SOD1) is implicated in causing neurodegeneration. Recent studies have suggested that destabilization and aggregation of the most immature form of SOD1, the disulfide-reduced, unmetallated (apo) protein is particularly important in causing ALS. We report herein in depth analyses of the effects of chemically and structurally diverse ALS-associated mutations on the stability and aggregation of reduced apo SOD1. In contrast with previous studies, we find that various reduced apo SOD1 mutants undergo highly reversible thermal denaturation with little aggregation, enabling quantitative thermodynamic stability analyses. In the absence of ALS-associated mutations, reduced apo SOD1 is marginally stable but predominantly folded. Mutations generally result in slight decreases to substantial increases in the fraction of unfolded protein. Calorimetry, ultracentrifugation, and light scattering show that all mutations enhance aggregation propensity, with the effects varying widely, from subtle increases in most cases, to pronounced formation of 40–100 nm soluble aggregates by A4V, a mutation that is associated with particularly short disease duration. Interestingly, although there is a correlation between observed aggregation and stability, there is minimal to no correlation between observed aggregation, predicted aggregation propensity, and disease characteristics. These findings suggest that reduced apo SOD1 does not play a dominant role in modulating disease. Rather, additional and/or multiple forms of SOD1 and additional biophysical and biological factors are needed to account for the toxicity of mutant SOD1 in ALS.

Mutations in Cu,Zn superoxide dismutase (SOD1) cause familial amyotrophic lateral sclerosis (fALS), a devastating and invariably fatal neurodegenerative disease. Although accounting for only a small percentage of all ALS cases, SOD1 mutations represent one of the main known causes of the disease. The similar symptoms and pathology of familial and sporadic ALS suggest common disease mechanisms and the potential for related therapeutic strategies (1–3). The mechanisms by which mutant SOD1 causes ALS are not known; however, extensive evidence supports a toxic gain of function due to increased aggregation of mutant protein. Misfolding and aggregation of diverse proteins are observed in numerous diseases, including other neurodegenerative diseases such as Alzheimer's, Huntington, and prion diseases (1, 2). Amyloid is a type of aggregate structure formed by many disease-associated proteins, and perhaps by all proteins, often under destabilizing conditions (4). Although there has been some controversy concerning the amyloid-like nature of large insoluble aggregates in mutant SOD1 mice models of ALS, amyloid aggregates are not observed in ALS patients (5–7). Here, we characterize the formation of small, soluble, nonamyloid aggregates by mutant SOD1.

In its mature form, SOD1 is a highly stable, homodimeric protein, with each subunit binding one catalytic copper ion and one structural zinc ion, and containing one intramolecular disulfide bond as well as two nonconserved free cysteines (Fig. S1*A*). Numerous in vivo and in vitro studies have shown that various immature, destabilized forms of SOD1 are prone to aggregate, and this is often enhanced by disease-associated mutations (8–16). Recently, attention has focused on aggregation of the most immature form of SOD1, in which the disulfide bond is reduced and no metals are bound (reduced apo). Studies of various mutant-SOD1 ALS mice models have shown that small, soluble, misfolded forms of reduced apo SOD1 are enriched in the spinal cord and may be the common cytotoxic species that cause ALS (17, 18). In addition, cell culture studies suggest that ALS-associated mutations can promote disulfide bond reduction and metal loss (19). Relatively little is known, though, about the properties of reduced apo SOD1, and how mutations affect these properties. In vitro studies have shown that agitation and/or oxidation of reduced apo SOD1 results in the formation of large, insoluble, amyloid aggregates (8, 10). However, the relevance of amyloid formation to ALS is questionable, and recent studies of mutant-SOD1 mice models have shown that formation of aberrant intermolecular disulfide bonds and large insoluble aggregates by SOD1 becomes pronounced only in the final, symptomatic stages of disease (13). There is also extensive evidence that smaller, soluble aggregates are particularly neurotoxic (2). Thus, it is of central importance to elucidate the properties of reduced apo SOD1s, and how these may relate to pathogenic mechanisms.

We report here in depth analyses of the effects of chemically and structurally diverse ALS-associated mutations on the stability and aggregation of reduced apo SOD1, under physiologically relevant quiescent, reducing conditions. The mutations are predominantly destabilizing, causing marked changes in the fraction of protein that is unfolded and increasing the propensity of the protein to form soluble aggregates. However, the formation of these aggregates is not well correlated with disease duration. Although the results suggest that aggregation of reduced apo SOD1 may play some role in disease, they do not support increased aggrega-

Author contributions: K.A.V., H.R.S., H.A.P., S.D.D., and E.M.M. designed research; K.A.V., H.R.S., H.A.P., M.S.T., S.M.S., R.S., and L.-A.K.B. performed research; S.P.S. and W.C. contributed new reagents/analytic tools; K.A.V., H.R.S., H.A.P., L.-A.K.B., S.D.D., and E.M.M. analyzed data; and K.A.V., H.R.S., H.A.P., and E.M.M. wrote the paper.

The authors declare no conflict of interest.

This article is a PNAS Direct Submission.

[1]K.A.V. and H.R.S. contributed equally to this work.

[2]Present address: Department of Biochemistry and Molecular Biology, University of Calgary, 2500 University Drive NW, Calgary, AB, Canada T2N 1N4.

[3]To whom correspondence should be addressed. E-mail: meiering@uwaterloo.ca.

This article contains supporting information online at www.pnas.org/lookup/suppl/doi:10.1073/pnas.0913021108/-/DCSupplemental.

tion of reduced apo mutants as the dominant determinant of ALS severity. Rather, multiple immature or aberrant forms of SOD1 are implicated in playing important roles in modulating disease.

Results

For most experiments herein, we employed a well-established pseudo WT (pWT) construct in order to facilitate measurements of stability and aggregation of reduced apo SOD1s and avoid complications caused by aberrant disulfide bond formation (8, 14–16, 20–22). In pWT, the nonconserved free cysteines at residues 6 and 111 are replaced by alanine and serine, respectively, whereas the highly conserved cysteines at residues 57 and 146 are retained (Fig. S1*A*). Cysteines 57 and 146 form a disulfide bond in mature forms of SOD1 but are reduced in the current study. pWT is a suitable background because its activity, structure, and stability are extremely similar to wild type, and use of this background formerly enabled thermodynamic stability analyses for disulfide-oxidized holo and apo SOD1s (15, 16, 23, 24). In various in vivo and in vitro studies, the free cysteines are frequently but not always observed to form aberrant disulfide bonds in aggregates, and they have been suggested to also play subtle roles in modulating noncovalent interactions during aggregation (8, 9, 11–14, 25). These effects were controlled for here by analyzing the properties of mutations relative to the pWT background in the absence of disulfide bond formation. In addition, we conducted some experiments using the WT background containing cysteines 6 and 111; the results obtained are consistent with those obtained using pWT.

All experiments on reduced apo SOD1s were conducted under physiologically relevant conditions of pH (20 mM Hepes, pH 7.4) and protein concentration (~30–60 μM monomer, 0.5–1.0 mg mL^{-1}) (11, 26), under reducing conditions [1 mM Tris(2-carboxyethyl)phosphine (TCEP)], with no agitation and sample incubation under anaerobic conditions. The reduced status of the protein throughout all experiments was confirmed by iodoacetamide modification of the reduced cysteines followed by SDS-PAGE (Fig. S1*B*) (11).

In the Absence of ALS-Associated Mutations, Reduced apo SOD1 Unfolds with High Reversibility at Well Above Physiological Temperature. The stability of reduced apo pWT and WT SOD1 were measured by differential scanning calorimetry (DSC) (Figs. 1 *A* and *B*, 2*D*, and Table S1), which shows that the temperature of maximum heat capacity (C_p), $t_{m,\mathrm{app}}$, is ~48 °C for both constructs. The $t_{m,\mathrm{app}}$ for reduced apo SOD1 is markedly lower compared to those for the more mature disulfide-oxidized apo and holo forms (Fig. 1*A*) (15, 16). However, despite being significantly less stable, reduced apo pWT thermally unfolds with high reversibility, typically ~95% (Fig. 1*B*), comparable to the reversibility for disulfide-oxidized forms of SOD1 (15, 23, 24). The reversibility for the WT (Fig. 2*D*) is somewhat lower, at ~75%, likely due to the presence of the free thiols that have been shown previously to decrease reversibility due to the formation of aberrant disulfide bonds (27). To minimize inaccuracies due to irreversibility, pWT was used for most of the further analyses.

Thermodynamic Analysis Under Physiologically Relevant Conditions Shows Reduced apo SOD1 Undergoes a Monomer Two-State Unfolding Transition and Is Predominantly Folded. High reversibility of unfolding is a prerequisite for thermodynamic analysis, which has not been reported previously for reduced apo SOD1. In previous studies, we showed that disulfide-oxidized apo and holo pWT SOD1 thermally unfold with high reversibility according to a two-state dimer unfolding mechanism (15); however, reduction or mutation of the disulfide bond in apo SOD1 greatly weakens the dimer interface (26, 28, 29). Measurements of thermal unfolding for reduced apo pWT are consistent with a monomer unfolding transition, showing no systematic shift in $t_{m,\mathrm{app}}$ over ~20-fold range in protein concentration (7–152 μM, 0.1–2.4 mg mL^{-1}) (Fig. S2*A*).

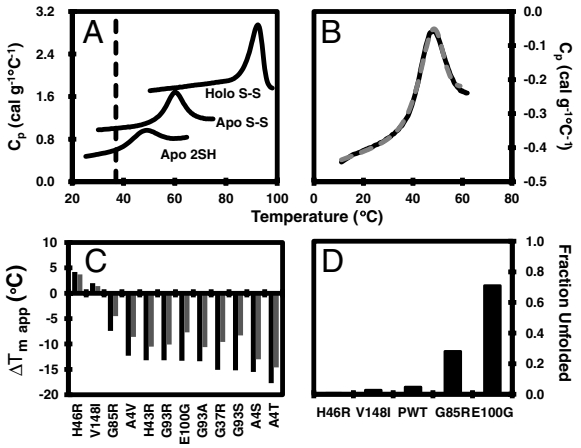

Fig. 1. Reversible thermal unfolding of reduced apo pWT SOD1. (*A*) DSC scans of pWT SOD1 in the reduced apo form in 20 mM Hepes, 1 mM TCEP, pH 7.4 and the disulfide-intact apo and holo forms in 20 mM Hepes, pH 7.8. The dashed black line indicates physiological temperature. (*B*) Consecutive thermal unfolding traces of disulfide-intact apo pWT SOD1 in which the sample was heated (solid black line), cooled and heated again (dashed gray line). (*C*) Change in apparent t_m of apo SOD1 in the disulfide-oxidized (light shaded bars) and the disulfide-reduced form (dark shaded bars). (*D*) Fraction of unfolded reduced apo mutant SOD1 at 37 °C, calculated from thermodynamic parameters (Table 1 and *SI Text*).

The unfolding data for pWT are well fit using a two-state monomer unfolding model (Table 1 and *SI Text*), with an average van't Hoff to calorimetric enthalpy ratio ($\Delta H_{\mathrm{vH}}/\Delta H_{\mathrm{cal}}$) of 1.1 ± 0.2 (Table 1 and Table S1), further confirming the applicability of the two-state monomer model (30). Similar fits are obtained for WT (Fig. 2*E*, Table 1, and Table S1).

Calculation of the temperature dependence of stability requires knowledge of the change in heat capacity upon unfolding, ΔC_p (*SI Text*), which was determined by Kirchoff analysis (31) to be 1.1 ± 0.1 kcal mol^{-1} °C^{-1} for reduced apo pWT (Fig. S2 *B* and *C*). This value is relatively low compared to that expected for a protein of this size, ~2 kcal mol^{-1} °C^{-1} (32, 33), suggesting that the reduced

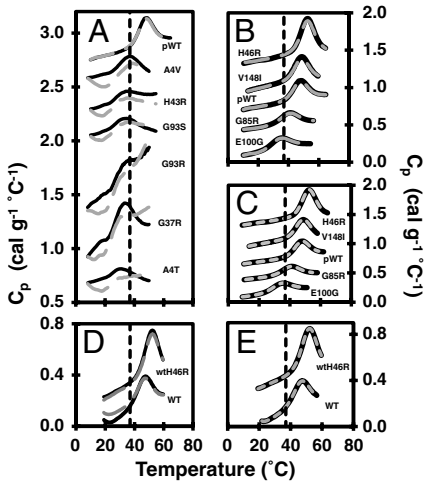

Fig. 2. Reversibility and data fitting of reduced apo mutants. The dashed black line indicates physiological temperature. (*A*) Consecutive thermal unfolding endotherms of reduced apo mutants with low unfolding reversibility and (*B*) with high unfolding reversibility (scan 1—solid black line; rescan—large dashed gray line). (*C*) DSC data fitting of the reduced apo mutants and pWT. Typical thermograms (solid black lines) with corresponding two-state monomer fits (small dashed gray lines) are shown. (*D*) Consecutive thermal unfolding endotherms of WT and wtH46R (scan 1—solid black line; rescan—large dashed gray line). (*E*) DSC data fitting of WT and wtH46R SOD1. Thermograms (solid black lines) with corresponding two-state monomer fits (small dashed gray lines) are shown. In each panel, the datasets are offset for clarity.

Table 1. Summary of thermodynamic parameters for reduced apo SOD1s

apo reduced SOD*	t_m, °C	ΔH_{vH}, kcal mol^{-1}	$\Delta H_{vH}/\Delta H_{cal}$	ΔC_p, kcal mol^{-1} °C^{-1}	ΔG,†,‡, 25 °C, kcal mol^{-1}	ΔG,† 37 °C, kcal mol^{-1}	$\Delta\Delta G$,§ 37 °C, kcal mol^{-1}
pWT	47.6 ± 0.5	50.5 ± 1.6	1.14 ± 0.15	0.72 ± 0.57	3.5 ± 0.1 *4.0 ± 0.2*	1.8 ± 0.1	N/A
H46R	52.6 ± 0.5	56.1 ± 4.2	0.95 ± 0.08	−0.42 ± 0.84	4.9 ± 0.1 *5.1 ± 0.1*	3.1 ± 0.1	+1.3
V148I	51.0 ± 1.1	58.4 ± 2.6	0.93 ± 0.04	−2.62 ± 1.19	3.6 ± 0.1	2.2 ± 0.0	+0.4
G85R	40.7 ± 0.4	46.9 ± 1.8	1.06 ± 0.36	−0.11 ± 0.34	2.1 ± 0.1	0.6 ± 0.0	−1.2
E100G	33.2 ± 1.2	47.3 ± 2.0	1.27 ± 0.06	0.79 ± 0.32	1.0 ± 0.1	−0.6 ± 0.2	−2.4
WT	46.8 ± 0.4	57.2 ± 1.1	1.49 ± 0.27	1.01 ± 0.67	3.0 ± 0.0	1.6 ± 0.0	N/A
wtH46R	52.7 ± 2.5	57.4 ± 5.4	0.76 ± 0.22	−1.59 ± 3.18	3.8 ± 0.5	2.4 ± 0.4	+0.8

N/A, not applicable.

All values are averages and standard deviations from at least three samples (Table S1), excluding WT and V148I, which are averaged over two samples.

*All mutants are in the pWT background unless otherwise specified.

†Values are calculated using the thermodynamic parameters obtained from the monomer two-state model and a temperature independent ΔC_p of 1.1 ± 0.1 kcal mol^{-1} °C^{-1} (Fig. 2 *B* and *C*).

‡Values in italics are from monomer two-state unfolding fits of equilibrium urea chemical denaturation curves (Fig. S2 *D* and *E*).

§$\Delta\Delta G = \Delta G_{(mutant)} - \Delta G_{(pWT)}$.

apo monomer may be less structured than a typical globular protein. The Gibbs free energy of unfolding, ΔG, calculated from the thermodynamic parameters is 3.5 ± 0.1 and 1.8 ± 0.1 kcal mol^{-1} at 25 °C and 37 °C, respectively (Table 1). Similar values were obtained for WT and are given in Table 1.

An independent measure of ΔG was obtained for pWT using CD-monitored equilibrium urea chemical denaturation and renaturation curves (Fig. S2 *D* and *E* and Table 1). These data are also well fit by a two-state monomer unfolding transition, giving a ΔG of 4.0 ± 0.2 kcal mol^{-1} at 25 °C, which is in reasonable agreement with the value obtained by DSC, and previous chemical denaturation experiments for reduced apo WT at pH 6.3 (29).

Knowledge of ΔG enables calculation of the fraction of protein that is unfolded, f_U (*SI Text*). For pWT at 37 °C, f_U is ∼0.05 (Fig. 1*D*), showing that the protein is predominantly (95%) folded. However, owing to the relatively low value of ΔG, f_U is very sensitive to small perturbations in stability caused by mutation, as described below.

DSC Reveals Complex Effects of ALS-Associated Mutations on the Stability and Aggregation Propensity of Reduced apo SOD1. The effects of chemically and structurally diverse ALS-associated SOD1 mutations on both the disulfide-oxidized and reduced apo forms of the protein were also analyzed by DSC. The mutations include A4V, T and S, and V148I, located in the dimer interface; G37R and H43R, affecting the packing of residues in the beta barrel; metal binding mutants H46R and G85R; G93R, S, A, and D at a mutational hot-spot within a tight turn; and E100G located at the end of strand 6, which eliminates a salt bridge with K30 (Fig. S1*A*). All of the mutants produced measurable thermograms (Fig. 2 *A* and *B* and Table S2), except G93D.

Based on lower $t_{m,app}$ values, the mutants are generally destabilized relative to pWT, except for H46R and V148I, which have slightly increased stabilities (Fig. 1*C* and Table S2). Furthermore, in the reduced apo form all mutants except H46R, V148I, and G85R have $t_{m,app}$ values at or below 37 °C (Table S2). This is in contrast to the more mature disulfide-oxidized apo form where the mutants all have $t_{m,app}$ values significantly higher than 37 °C (15, 24). Although it is difficult to directly compare the effects of the mutations on the thermodynamic stability of the oxidized to the reduced apo forms due to the change in quaternary structure, it is noteworthy that the changes in melting temperature are larger in the reduced apo form compared to the oxidized apo form (Fig. 1*C* and Table S2). Similarly, the effects of mutations in nonmetal binding mutants are larger in the oxidized apo forms than in the holo (metallated) forms (15), suggesting that the effects of mutations in SOD1 tend to propagate more as the protein becomes increasingly destabilized and folding becomes less cooperative. Overall, the propensity of most reduced apo SOD1s to misfold/aggregate is evident from the decreased reversibility of thermal unfolding traces (Fig. 2*A*), which is generally most pronounced in the significantly destabilized mutants.

Nevertheless, the reversibility of thermal unfolding is remarkably high for several mutants: H46R, V148I, G85R, and E100G, enabling thermodynamic analysis using the two-state monomer unfolding model (Fig. 2 *B* and *C*, Table 1, and Table S1). Similar results were also obtained for H46R in the WT background (Fig. 2 *D* and *E*, Table 1, and Table S1). The stability of pWT and H46R was also measured using chemical denaturation, again giving results consistent with those obtained by DSC (Fig. S2 *D* and *E* and Table 1). Using the fitted thermodynamic parameters, f_U at 37 °C is calculated to be 0.05, 0.007, 0.03, 0.28, and 0.71 for pWT, H46R, V148I, G85R, and E100G, respectively (Fig. 1*D* and *SI Text*). Thus, at physiological temperature the slightly stabilizing H46R and V148I mutants are predominantly folded (in fact, more so than pWT), but the proportion of unfolded protein is markedly increased for the other destabilizing mutants, with E100G being more unfolded than folded. This differs significantly from the effects of the mutations in the disulfide-oxidized apo form where the proteins remain very predominantly folded (Table S2) (24).

Although the thermal unfolding of these reduced apo SOD1s is highly reversible, there is some evidence in the DSC fitted parameters for increased aggregation propensity (15). H46R, G85R, and V148I have relatively low, mostly negative, fitted ΔC_ps, with average values of -0.42 ± 0.84, -2.62 ± 1.19, and -0.11 ± 0.34 kcal mol^{-1} °C^{-1}, respectively (Table 1). The negative average ΔC_ps for H46R and V148I is pronounced and consistent, suggesting the occurrence of exothermic aggregation as these mutants thermally unfold (15). In contrast, E100G does not exhibit unusually low ΔC_p values; however, the $\Delta H_{vH}/\Delta H_{cal}$ ratios tend to be larger than 1 (1.3 ± 0.1 on average), suggesting a larger cooperative unfolding unit, i.e., presence of aggregates (34). Overall, the DSC data are suggestive of subtle increases in aggregation of all mutant SOD1s.

Analytical Ultracentrifugation Shows That Reduced apo SOD1s Are Predominantly Monomeric, and Mutations Slightly Increase Protein–Protein Interactions. In order to further investigate the tendency of reduced apo SOD1s to aggregate, analytical ultracentrifugation (AUC) sedimentation velocity and equilibrium experiments were performed (*SI Text*). Sedimentation velocity experiments can assess sample heterogeneity with high sensitivity. Analysis of the velocity data for pWT and H43R revealed species with sedimentation coefficients of 1.5–2 S (Fig. S3), very similar to the values reported previously for reduced apo WT SOD1 (28). The plots of boundary fraction versus sedimentation coefficient show only a modest slope, indicating no significant population of dimers or larger aggregated species for either pWT or H43R in these experiments.

Sedimentation equilibrium experiments at several rotor speeds (20,000, 25,000, 30,000, and 35,000 rpm) were also performed to analyze the molecular weights (MWs) of the species present in solution. Fitting of the equilibrium data for pWT, H43R, A4V,

and E100G to a single species model gave highly reproducible results (Table S3). For the pWT protein, the fitted MW at lower rotor speeds is generally close to 15 kDa, just under the calculated mass of ~15.8 kDa. In contrast to the pWT, the fitted MWs for the A4V and E100G mutants are intermediate between monomer and dimer, whereas fits for the mutant H43R tend to give values closer to what would be expected for a dimer. Additionally, fitted MW values for all mutants markedly decrease with increased rotor speed (Table S3). These results clearly indicate increased intermolecular association of the mutant proteins. Attempts to fit the data to two-state models for monomer/dimer, monomer/trimer, and monomer/tetramer transitions gave poor fits with nonrandom residuals, indicating that the association is likely more complex than a simple two-state process. Overall, the sedimentation equilibrium data indicate that the pWT protein remains predominantly monomeric during the lengthy period required for these studies, but that the mutants have an increased tendency to form small aggregated species. These findings are consistent with the results of the DSC experiments.

Light Scattering Reveals Marked Differences in Aggregation of Mutants upon Prolonged Incubation. Dynamic light scattering (DLS) was used to monitor the size of particles in solution upon incubating samples at 37 °C (Fig. 3 and Figs. S4 and S5*A*). It is important to note that light scattering intensity is proportional to the sixth power of the diameter of the scattering particle; thus this technique is extremely sensitive to aggregate formation (35). DLS analyses showed that all reduced apo SOD1 solutions were initially monodisperse, with a single species of hydrodynamic diameter ~5–6 nm. This diameter is intermediate between those expected for a protein the size of SOD1 in the fully folded and unfolded states (36), consistent with the relatively low ΔC_p (see above), and suggesting that the folded reduced apo SOD1 may have an expanded structure.

Upon prolonged incubation, gradual formation of small amounts of soluble aggregates was observed, with distinct differences between mutants (Fig. 3 and Figs. S4 and S5). At one extreme, H46R and V148I show only very slight evidence for aggregation, with more than 99% of the protein remaining as reduced monomers after ~300 h of incubation (Fig. 3*D* and S4*D*). In contrast, A4V and H43R show the most pronounced evidence of soluble aggregates species (Fig. 3 *C* and *F*). A4V forms aggregates with hydrodynamic diameters of 40–60 nm within ~15 h of incubation, and these approximately double in diameter and increase in abundance over ~2 weeks. H43R forms 100–1,000 nm species within ~60 h, which also increase in abundance with time. For both mutants, at long incubation times the larger species dominate the scattering and the soluble monomers can no longer be observed. However, the total intensity of scattered light continues to increase, indicating continued aggregation (Fig. S5*B*). In general, the extent of aggregation of different mutants, as shown by the prominence of large species in the size distributions (Fig. 3 and Figs. S4 and S5*A*), is consistent with the extent of aggregation as indicated by total light scattering intensity (Fig. S5 *B–D*). Both observations give similar indications of the relative aggregation propensities of different mutants. It should be noted, however, that lack of observation of the monomer peak does not indicate a predominantly aggregated sample. If one considers a hypothetical mixture containing only 5- and 50-nm species, due to the dependence of light scattering intensity on the sixth power of the diameter, when 99% of the intensity arises from the 50-nm species, this species will account for only 0.1% by mass of the total protein in solution (35). Therefore, the DLS data indicate only slight to moderate formation of soluble aggregates by reduced apo SOD1 variants, consistent with the DSC and centrifugation data.

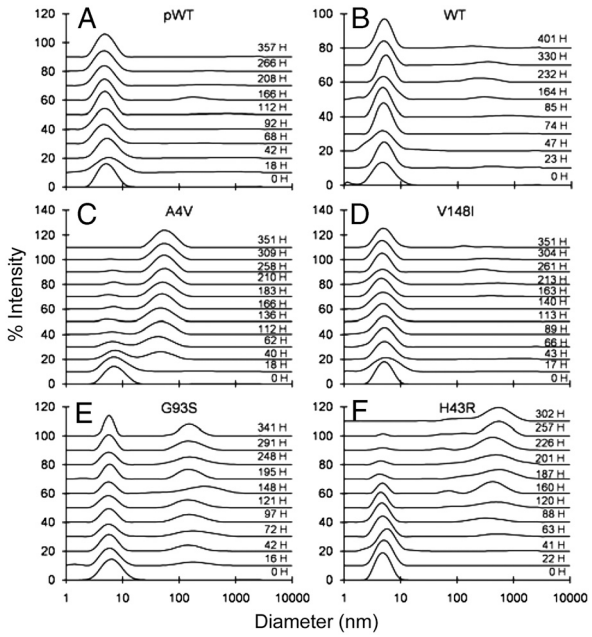

Fig. 3. Particle size distributions for reduced apo pWT and mutants at 37 °C, pH 7.4 measured by dynamic light scattering over time, as indicated in hours (H).

Discussion

The biophysical analyses conducted here show that ALS-associated mutations have the most pronounced effects on stability in the reduced apo form of SOD1 and enhance the formation of soluble aggregates. These represent unique in-depth analyses of reduced apo SOD1 stability and aggregation, and they have important implications for understanding mechanisms of SOD1 aggregation that may be involved in ALS, considered further below.

In the Absence of ALS-Associated Mutations, Reduced apo SOD1 Is Predominantly Folded and Has Low Aggregation Propensity Under Physiologically Relevant Conditions. The unfolding of pWT measured here by DSC and chemical denaturation is well fit by a reversible two-state monomer unfolding transition, based on multiple DSC and chemical denaturation criteria (Fig. 2*C*, Fig. S2 *D* and *E*, and Table 1), and comparable results are obtained by DSC for WT (Fig. 2*E* and Table 1). These results reveal that the ΔG of unfolding for reduced apo SOD1 at 37 °C, which has not been reported previously, is 1.8 ± 0.1 kcal mol^{-1} for pWT and 1.6 ± 0.0 kcal mol^{-1} for WT. Thus, at physiological temperature and pH, the protein is predominantly folded and shows very little tendency to aggregate.

The very minimal aggregation observed here for monomeric reduced apo pWT and WT is particularly noteworthy given that previous studies have reported monomerization and loss of metals greatly enhance, or are required for, aggregation (8, 37). Moreover, several studies have reported observations of amyloid formation by apo SOD1 in which the intramolecular disulfide bond was reduced or removed by mutagenesis (8, 10, 14). A key difference between these and the current studies is their use of agitation rather than quiescent solution conditions. It is well established that agitation promotes the aggregation of many proteins, often as amyloid (8, 38, 39). This is not well understood but likely involves interface effects and perhaps also accelerated oxidation of free thiols.

The relevance of the formation of amyloid aggregates in previous studies of reduced apo SOD1 to ALS disease mechanisms is not clear. Other forms of SOD1 have also been shown previously to form amyloid under destabilizing conditions caused by denaturant, sonication, trifluoroethanol, or low pH (8, 14, 20, 40), and formation of intermolecular disulfide bonds (25). In contrast, other studies under less extreme conditions have also reported evidence for distinct aggregation processes from native-like states (41–43). Protein aggregation is generally strongly dependent on solution conditions, and many destabilizing and often nonphysiological conditions can result in the formation of amyloid. In this regard, it should be noted that the amyloid-specific characteristic

of green–gold Congo red birefringence and ThT binding of aggregates is not observed in ALS (5, 7) and the intracellular SOD1-containing aggregates in fALS have a granule-coated rather than the smooth fibrillar structure characteristic of amyloid (6); thus, ALS is not a typical amyloid disease.

A key aspect for in vitro studies of aggregation is to consider their relation to in vivo conditions. Here we have used physiologically relevant conditions of temperature, pH, protein concentration, and quiescence. Importantly, the very minimal aggregation of reduced apo pWT and WT is consistent with cell culture and mice studies where wild-type SOD1 shows very little tendency to aggregate and mice do not develop ALS symptoms (13, 17). This differs from observations for mutant SOD1s, which tend to aggregate more than WT in cell culture and form small aggregated species in mice prior to the onset of symptoms followed by large disulfide-linked aggregates in the final stages of disease (12, 13). In contrast, in previous in vitro studies the comparable wild-type-like constructs not only formed amyloid (8, 10, 14) but in some cases this was more pronounced than for ALS-associated mutants (10). This suggests fundamentally different aggregation processes are being observed under different conditions.

ALS-Associated Mutations Have Complex Effects on Stability and Aggregation. Under the physiologically relevant conditions used herein, we were able to measure the effects of many chemically and structurally diverse ALS-associated mutations on stability and aggregation propensity. The effects on stability range from slightly stabilizing to slightly or significantly destabilizing (Fig. 1*C*, Table 1, and Table S2). Consistent with previous studies on apo SOD1 where metal binding mutations had relatively small effects on $t_{m,\mathrm{app}}$ (44), the metal binding mutants H46R and G85R are among the most stable mutants studied here. In the disulfide-oxidized apo form, all the mutants have $t_{m,\mathrm{app}}$ values well above physiological temperature; however, in the reduced apo form, most have $t_{m,\mathrm{app}}$ values close to or lower than 37 °C, indicating that they will be 50% or more unfolded at physiological temperature (Fig. 1*D* and Table S2). The observation that decreases in melting temperatures tend to be largest in the reduced apo form implies that substantial increases in the population of unfolded conformations will also occur for many other mutants that have been found to have decreased $t_{m,\mathrm{app}}$ in the disulfide-oxidized apo form (15, 24, 44). Thus, overall, many but not all ALS-associated mutations are likely to significantly increase the population of reduced apo unfolded monomers.

Regardless of stability, the DSC, AUC, and DLS experiments indicate that the reduced apo mutants generally have increased propensity to misfold/aggregate. In particular, DLS results indicate that distinct sizes of small, soluble aggregates are observed for different mutants (Fig. 3 and Figs. S4 and S5*A*). Evidence for structural polymorphism of SOD1 aggregates was also reported for agitation-induced aggregation (26). These findings are intriguing as variations in aggregate structures may cause different disease phenotypes.

Limited Correlations Between the Properties of Reduced apo Mutant SOD1s and ALS Characteristics Implicate Multiple Forms of SOD1 in Modulating Disease. Correlations between the properties of mutant SOD1 and ALS disease characteristics have been sought for many years and are critical for deciphering disease mechanisms. Previous studies have reported evidence for a weak inverse correlation between oxidized apo SOD1 stability and ALS disease duration (45–47), which improves when global or local protein characteristics such as charge (48) or hydrogen bonding (45) are considered. The results for V148I suggest that increased hydrophobicity of the exposed dimer interface may be another significant modulator of aggregation. A weak correlation is observed between reduced apo mutant SOD1 stability and disease duration (Fig. 4 and Fig. S6*A*), suggesting that the effects of the mutations on the stability of reduced apo SOD1 do not play a more significant role than their effects in oxidized apo in determining disease duration. This implies that factors beyond stability, and multiple forms of SOD1, are important in modulating disease duration.

There is a significant correlation ($r = 0.78$, Fig. 4 and Fig. S6*B*) between observed aggregation and mutant destabilization, consistent with results of general studies of protein aggregation. This has also been observed for more mature forms of SOD1 that tend to aggregate more readily when destabilized (10, 11, 15, 16). The aggregation observed here is poorly correlated with nine different aggregation prediction models (Fig. S6*E* and *SI Text*). The lack of correlations may be because most of these prediction algorithms were developed based on datasets of amyloid-forming proteins and peptides. As noted above, amyloid formation may differ significantly from the formation of the soluble, nonamyloid aggregates that are characterized here. There is also no significant correlation between observed aggregation and ALS disease duration (Fig. 4 and Fig. S6*C*). Furthermore, the aggregation propensities of the SOD1 mutants predicted using the preceding methods are also poorly correlated with disease duration (Fig. S6*D*).

Consideration of these correlations points to two key conclusions: Neither the association of reduced apo SOD1 mutants into small soluble aggregates nor the predicted aggregation propensities of SOD1 mutants are able to account for fALS disease duration. These key findings have two important implications: (*i*) Multiple forms of SOD1 are likely to modulate disease characteristics and (*ii*) amyloid formation is likely not an important factor in SOD1-associated fALS. Further support for the first point is evidence that mutations enhance the population and aggregation of various immature forms of mutant SOD1, and the observation of multiple forms of SOD1 in aggregates in vivo (1, 13, 15, 16, 21, 41, 42, 49). The second point is further supported by evidence that fALS patient data fail to reveal any support for a role of amyloid in disease (7).

In conclusion, the results reported here provide unique and important data on the stability and aggregate formation by reduced apo SOD1s, which should prove useful for further testing of ALS disease hypotheses. The increased aggregation of reduced apo SOD1 upon mutation suggests that this form of the protein may play a role in causing disease. However, the lack of strong correlations between reduced apo SOD1 stability and disease duration and between measured aggregation and disease duration imply that the effects of mutations on reduced apo SOD1 are unlikely to be the dominant factor in modulating disease, and that multiple forms of the protein are involved. Unravelling the complex aggregation processes that are likely to contribute to the syndrome of ALS (50) may ultimately lead to new and urgently needed approaches for treating this devastating disease.

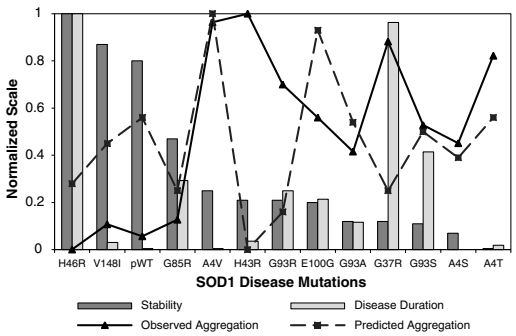

Fig. 4. A correlation plot representing the relationship between reduced apo SOD1 mutant stability, fALS disease durations, and observed and predicted aggregation. The stability is determined by a change in apparent t_m of mutants compared to pWT and normalized, from 0 (least stable) to 1 (most stable). Observed aggregation is based on DLS measurements as described in Fig. S5*A*. Predicted aggregation based on the Chiti et al. method (52) was normalized from 0 (lowest propensity) to 1 (highest propensity). Disease duration (47) is normalized from 0 (short) to 1 (long).

Materials and Methods

Expression and Purification of Mutant SOD1. Disulfide-oxidized apo SOD1 proteins were prepared as described previously (24, 51). Reduced apo SOD1 was prepared by first unfolding the protein in 2 M GdmCl, 20 mM Hepes, pH 7.8 for 30 min at ambient temperature with degassing. Tris(2-carboxyethyl)phosphine hydrochloride (TCEP.HCl) was then added to a final concentration of 10 mM with reduction occurring in an anaerobic environment for 1 h. Finally, samples were exchanged into buffer containing 1 mM TCEP.HCl, 20 mM Hepes pH 7.4 by successive dilutions and reconcentrations using a 3-kDa cutoff Nanosep centrifugal device (Pall Corporation).

Differential Scanning Calorimetry. DSC scans of apo SOD1 samples were performed as described elsewhere (15). After subtraction of buffer versus buffer scans from protein versus buffer scans, disulfide-reduced apo SOD1 data were fit to a two-state monomer unfolding model after normalizing for protein concentration (*SI Text*).

Light Scattering Measurements. Time average dynamic light scattering measurements were performed using a Zetasizer Nano ZS (Malvern Instruments Ltd.). Particle size was determined from an average of three correlation functions, each being the average of five consecutive 10-s data accumulations. Particle size was analyzed by the CONTIN method using Malvern software. Samples were initially measured daily and then at increasing time intervals.

ACKNOWLEDGMENTS. We are grateful to Gian Tartaglia for assistance in using Zyggregator and Joost Schymkowitz for helpful correspondence regarding the Tango and Waltz algorithm. We thank the ALS Society of Canada, Muscular Dystrophy Canada, and Canadian institutes of Health Research for funding this research.

1. Turner BJ, Talbot K (2008) Transgenics, toxicity and therapeutics in rodent models of mutant SOD1-mediated familial ALS. *Prog Neurobiol* 85:94–134.
2. Soto C, Estrada LD (2008) Protein misfolding and neurodegeneration. *Arch Neurol* 65:184–189.
3. Boillee S, Vande Velde C, Cleveland DW (2006) ALS: A disease of motor neurons and their nonneuronal neighbors. *Neuron* 52:39–59.
4. Fandrich M, et al. (2003) Myoglobin forms amyloid fibrils by association of unfolded polypeptide segments. *Proc Natl Acad Sci USA* 100:15463–15468.
5. Okamoto K, Hirai S, Yamazaki T, Sun XY, Nakazato Y (1991) New ubiquitin-positive intraneuronal inclusions in the extra-motor cortices in patients with amyotrophic lateral sclerosis. *Neurosci Lett* 129:233–236.
6. Kato S, et al. (2000) New consensus research on neuropathological aspects of familial amyotrophic lateral sclerosis with superoxide dismutase 1 (SOD1) gene mutations: Inclusions containing SOD1 in neurons and astrocytes. *Amyotroph Lateral Sc* 1:163–184.
7. Kerman A, et al. (2010) Amyotrophic lateral sclerosis is a non-amyloid disease in which extensive misfolding of SOD1 is unique to the familial form. *Acta Neuropathol* 119:335–344.
8. Chattopadhyay M, et al. (2008) Initiation and elongation in fibrillation of ALS-linked superoxide dismutase. *Proc Natl Acad Sci USA* 105:18663–18668.
9. Cozzolino M, et al. (2008) Cysteine 111 affects aggregation and cytotoxicity of mutant Cu,Zn-superoxide dismutase associated with familial amyotrophic lateral sclerosis. *J Biol Chem* 283:866–874.
10. Furukawa Y, Kaneko K, Yamanaka K, O'Halloran TV, Nukina N (2008) Complete loss of post-translational modifications triggers fibrillar aggregation of SOD1 in the familial form of amyotrophic lateral sclerosis. *J Biol Chem* 283:24167–24176.
11. Furukawa Y, O'Halloran TV (2005) Amyotrophic lateral sclerosis mutations have the greatest destabilizing effect on the apo- and reduced form of SOD1, leading to unfolding and oxidative aggregation. *J Biol Chem* 280:17266–17274.
12. Karch CM, Borchelt DR (2008) A limited role for disulfide cross-linking in the aggregation of mutant SOD1 linked to familial amyotrophic lateral sclerosis. *J Biol Chem* 283:13528–13537.
13. Karch CM, Prudencio M, Winkler DD, Hart PJ, Borchelt DR (2009) Role of mutant SOD1 disulfide oxidation and aggregation in the pathogenesis of familial ALS. *Proc Natl Acad Sci USA* 106:7774–7779.
14. Oztug Durer ZA, et al. (2009) Loss of metal ions, disulfide reduction and mutations related to familial ALS promote formation of amyloid-like aggregates from superoxide dismutase. *PLoS ONE* 4:e5004.
15. Stathopulos PB, et al. (2006) Calorimetric analysis of thermodynamic stability and aggregation for apo and holo amyotrophic lateral sclerosis-associated Gly-93 mutants of superoxide dismutase. *J Biol Chem* 281:6184–6193.
16. Stathopulos PB, et al. (2003) Cu/Zn superoxide dismutase mutants associated with amyotrophic lateral sclerosis show enhanced formation of aggregates in vitro. *Proc Natl Acad Sci USA* 100:7021–7026.
17. Wang J, et al. (2009) Progressive aggregation despite chaperone associations of a mutant SOD1-YFP in transgenic mice that develop ALS. *Proc Natl Acad Sci USA* 106:1392–1397.
18. Zetterstrom P, et al. (2007) Soluble misfolded subfractions of mutant superoxide dismutase-1 s are enriched in spinal cords throughout life in murine ALS models. *Proc Natl Acad Sci USA* 104:14157–14162.
19. Tiwari A, Hayward LJ (2003) Familial amyotrophic lateral sclerosis mutants of copper/zinc superoxide dismutase are susceptible to disulfide reduction. *J Biol Chem* 278:5984–5992.
20. DiDonato M, et al. (2003) ALS mutants of human superoxide dismutase form fibrous aggregates via framework destabilization. *J Mol Biol* 332:601–615.
21. Valentine JS, Doucette PA, Potter SZ (2005) Copper-zinc superoxide dismutase and amyotrophic lateral sclerosis. *Annu Rev Biochem* 74:563–593.
22. Svensson AK, Bilsel O, Kondrashkina E, Zitzewitz JA, Matthews CR (2006) Mapping the folding free energy surface for metal-free human Cu,Zn superoxide dismutase. *J Mol Biol* 364:1084–1102.
23. Rumfeldt JA, Stathopulos PB, Chakrabarrty A, Lepock JR, Meiering EM (2006) Mechanism and thermodynamics of guanidinium chloride-induced denaturation of ALS-associated mutant Cu,Zn superoxide dismutases. *J Mol Biol* 355:106–123.
24. Vassall KA, Stathopulos PB, Rumfeldt JA, Lepock JR, Meiering EM (2006) Equilibrium thermodynamic analysis of amyotrophic lateral sclerosis-associated mutant apo Cu,Zn superoxide dismutases. *Biochemistry* 45:7366–7379.
25. Banci L, et al. (2007) Metal-free superoxide dismutase forms soluble oligomers under physiological conditions: A possible general mechanism for familial ALS. *Proc Natl Acad Sci USA* 104:11263–11267.
26. Arnesano F, et al. (2004) The unusually stable quaternary structure of human Cu,Zn-superoxide dismutase 1 is controlled by both metal occupancy and disulfide status. *J Biol Chem* 279:47998–48003.
27. Lepock JR, Frey HE, Hallewell RA (1990) Contribution of conformational stability and reversibility of unfolding to the increased thermostability of human and bovine superoxide dismutase mutated at free cysteines. *J Biol Chem* 265:21612–21618.
28. Doucette PA, et al. (2004) Dissociation of human copper-zinc superoxide dismutase dimers using chaotrope and reductant. Insights into the molecular basis for dimer stability. *J Biol Chem* 279:54558–54566.
29. Lindberg MJ, Normark J, Holmgren A, Oliveberg M (2004) Folding of human superoxide dismutase: Disulfide reduction prevents dimerization and produces marginally stable monomers. *Proc Natl Acad Sci USA* 101:15893–15898.
30. Sturtevant JM (1987) Biochemical applications of differential scanning calorimetry. *Annu Rev Phys Chem* 38:463–488.
31. Privalov PL (1979) Stability of proteins: Small globular proteins. *Adv Protein Chem* 33:167–241.
32. Geierhaas CD, Nickson AA, Lindorff-Larsen K, Clarke J, Vendruscolo M (2007) BPPred: A Web-based computational tool for predicting biophysical parameters of proteins. *Protein Sci* 16:125–134.
33. Myers JK, Pace CN, Scholtz JM (1995) Denaturant m values and heat capacity changes: Relation to changes in accessible surface areas of protein unfolding. *Protein Sci* 4:2138–2148.
34. Privalov PL, Potekhin SA (1986) Scanning microcalorimetry in studying temperature-induced changes in proteins. *Methods Enzymol* 131:4–51.
35. Lomakin A, Benedek GB, Teplow DB (1999) Monitoring protein assembly using quasielastic light scattering spectroscopy. *Methods Enzymol* 309:429–459.
36. Wilkins DK, et al. (1999) Hydrodynamic radii of native and denatured proteins measured by pulse field gradient NMR techniques. *Biochemistry* 38:16424–16431.
37. Khare SD, Caplow M, Dokholyan NV (2004) The rate and equilibrium constants for a multistep reaction sequence for the aggregation of superoxide dismutase in amyotrophic lateral sclerosis. *Proc Natl Acad Sci USA* 101:15094–15099.
38. Kiese S, Papppenberger A, Friess W, Mahler HC (2008) Shaken, not stirred: Mechanical stress testing of an IgG1 antibody. *J Pharm Sci* 97:4347–4366.
39. Yamamoto K, et al. (2008) Thiol compounds inhibit the formation of amyloid fibrils by beta 2-microglobulin at neutral pH. *J Mol Biol* 376:258–268.
40. Stathopulos PB, et al. (2004) Sonication of proteins causes formation of aggregates that resemble amyloid. *Protein Sci* 13:3017–3027.
41. Elam JS, et al. (2003) Amyloid-like filaments and water-filled nanotubes formed by SOD1 mutant proteins linked to familial ALS. *Nat Struct Biol* 10:461–467.
42. Banci L, et al. (2005) Fully metallated S134N Cu,Zn-superoxide dismutase displays abnormal mobility and intermolecular contacts in solution. *J Biol Chem* 280:35815–35821.
43. Hwang YM, et al. (2010) Non-amyloid aggregates arising from mature Cu/Zn superoxide dismutases resemble those observed in amyotrophic lateral sclerosis. *J Biol Chem* 285:41701–41711.
44. Rodriguez JA, et al. (2005) Destabilization of apoprotein is insufficient to explain Cu,Zn-superoxide dismutase-linked ALS pathogenesis. *Proc Natl Acad Sci USA* 102:10516–10521.
45. Bystrom R, Andersen PM, Grobner G, Oliveberg M (2010) SOD1 mutations targeting surface hydrogen bonds promote amyotrophic lateral sclerosis without reducing apo-state stability. *J Biol Chem* 285:19544–19552.
46. Lindberg MJ, Bystrom R, Boknas N, Andersen PM, Oliveberg M (2005) Systematically perturbed folding patterns of amyotrophic lateral sclerosis (ALS)-associated SOD1 mutants. *Proc Natl Acad Sci USA* 102:9754–9759.
47. Wang Q, Johnson JL, Agar NY, Agar JN (2008) Protein aggregation and protein instability govern familial amyotrophic lateral sclerosis patient survival. *PLoS Biol* 6:e170.
48. Sandelin E, Nordlund A, Andersen PM, Marklund SS, Oliveberg M (2007) Amyotrophic lateral sclerosis-associated copper/zinc superoxide dismutase mutations preferentially reduce the repulsive charge of the proteins. *J Biol Chem* 282:21230–21236.
49. Hayward LJ, et al. (2002) Decreased metallation and activity in subsets of mutant superoxide dismutases associated with familial amyotrophic lateral sclerosis. *J Biol Chem* 277:15923–15931.
50. Turner MR, Kiernan MC, Leigh PN, Talbot K (2009) Biomarkers in amyotrophic lateral sclerosis. *Lancet Neurol* 8:94–109.
51. Lynch SM, Boswell SA, Colon W (2004) Kinetic stability of Cu/Zn superoxide dismutase is dependent on its metal ligands: Implications for ALS. *Biochemistry* 43:16525–16531.
52. Chiti F, Stefani M, Taddei N, Ramponi G, Dobson CM (2003) Rationalization of the effects of mutations on peptide and protein aggregation rates. *Nature* 424:805–808.

Supporting Information

Vassall et al. 10.1073/pnas.0913021108

SI Materials and Methods.

Analysis of Differential Scanning Calorimetry (DSC) Thermal Unfolding Data. Thermal unfolding scans for reduced apo superoxide dismutase (SOD1) were fit to a two-state monomer unfolding model ($N \leftrightarrow U$) using the following Eq. **S1** (1):

$$C_p(T) = (A + BT)(1 - f_u) + (C + DT)f_u + \frac{\beta \Delta h^2(T) f_u (1 - f_u)}{\mathrm{RT}^2}, \quad \textbf{[S1]}$$

where $C_p(T)$ is the total specific heat capacity, normalized per gram of protein, at temperature, T (in Kelvin), f_u is the fraction of unfolded protein at T, R is the universal gas constant, $\Delta h(T)$ is the specific enthalpy of unfolding at T, A and B are the intercept and slope of the native baseline, respectively, whereas C and D are the intercept and slope of the unfolded baseline, respectively. β is a temperature-independent constant equal to the molecular weight of the dimer multiplied by the ratio of van't Hoff to calorimetric enthalpies of unfolding, $\Delta H_{\mathrm{vH}}/\Delta H_{\mathrm{cal}}$. The DSC data were fit to the approximate end of the unfolding transition due to the occurrence of downward sloping posttransition baselines, presumably due to exothermic aggregation of the unfolded protein at higher temperatures.

The baselines for scans obtained in urea for the determination of the change in heat capacity upon unfolding, ΔC_p, had higher variability, which created problems in obtaining consistent fitted values using Eq. **S1**. Accordingly, scans in urea were analyzed using the commonly employed baseline subtraction with linear connect (which effectively removes the influence of the baselines), followed by fitting of the resulting excess specific heat capacity, $C_p^{ex}(T)$, normalized per mol of protein, to the MN2-state model, Eq. **S2** (Microcal Origin version 5.0) (2–5):

$$C_p^{ex}(T) = \frac{\gamma \Delta H^2(T) f_u (1 - f_u)}{\mathrm{RT}^2}, \quad \textbf{[S2]}$$

where $\Delta H(T)$ is the enthalpy of unfolding at T, f_u is the fraction of unfolded protein, and γ is $\Delta H_{\mathrm{vH}}/\Delta H_{\mathrm{cal}}$. Fitted parameters for reduced apo pWT datasets acquired in the absence of urea gave fitted parameters that were very similar to those obtained using Eq. **S1** [<0.5 °C difference for t_m (temperature in °C at which $f_u = 0.5$) and <10% difference for ΔH_{vH} and ΔH_{cal}].

The fraction of unfolded protein can be determined from the equilibrium constant, $K(t)$, at temperature, t (°C) using Eq. **S3** and Eq. **S4**:

$$f_u = \frac{-1 + \sqrt{1 + \frac{8}{b}}}{\frac{4}{b}}, \quad \textbf{[S3]}$$

where

$$b = \frac{K(t)}{K(t_m)}. \quad \textbf{[S4]}$$

Calculation of Thermodynamic Parameters at 37 °C. $\Delta H(T)$, $\Delta S(T)$, and $\Delta G(T)$ of thermal unfolding were calculated at 37 °C (310.15 K) using a temperature independent ΔC_p as previously described (6) using the following equations:

$$\Delta G(T) = \Delta H(T) - T\Delta S(T), \quad \textbf{[S5]}$$

$$\Delta H(T) = \Delta H(T_m) - \Delta C_p(310.15 - T_m), \quad \textbf{[S6]}$$

$$\Delta S(T) = \Delta S(T_m) + \Delta C_p \ln\left(\frac{310.15}{T_m}\right), \quad \textbf{[S7]}$$

$$\Delta S(T_m) = \frac{\Delta H(T_m) + \Delta G(T_m)}{T_m}, \quad \textbf{[S8]}$$

and

$$\Delta G(T_m) = -\mathrm{R}T_m \ln P, \quad \textbf{[S9]}$$

where P is the protein concentration of monomer subunits and T_m is the temperature at which the protein is half unfolded.

Analytical Ultracentrifugation. Sedimentation velocity and equilibrium experiments were conducted at the Biomolecular Interactions & Conformations Facility (Shuclich School of Medicine & Dentistry, University of Western Ontario) using an Optima XL-A Analytical Ultracentrifuge (Beckman Coulter Inc.) with an An60Ti rotor and 2/6-channel cells with Epon-charcoal centerpieces. Centrifugation was carried out at 20 °C, 20 mM Hepes, 1 mM Tris(2-carboxyethyl)phosphine (TCEP), pH 7.4, with absorbance detection at either 252 or 280 nm. Equilibrium data were collected in radial step sizes of 0.002 cm and averaged over 10 readings. Equilibrium data were fit to a single ideal species model (see below) using Prism 5 (GraphPad Software).

Analysis of Sedimentation Equilibrium Data. Data were analyzed according to a single ideal species model as described elsewhere (7), according to Eq. **S10**:

$$A = A_o \exp\left[\frac{\omega^2}{2\mathrm{RT}} MW_{\mathrm{obs}}(1 - \bar{\nu}\rho)(x^2 - x_o^2)\right] + I_0, \quad \textbf{[S10]}$$

where A is the absorbance at radius x, A_o is the absorbance at reference radius x_o, ω is the angular velocity of the rotor, MW_{obs} is the fitted molecular weight of the protein, $\bar{\nu}$ is the partial specific volume of the protein, ρ is the density of the solvent, and I_o is the baseline offset.

Chemical Renaturation and Denaturation. Chemical renaturation and denaturation equilibrium curves of reduced apo SOD1 were prepared as described elsewhere (8), except that urea was used as the denaturant instead of guanidinium chloride. All samples contained 1 mM TCEP, 20 mM Hepes, pH 7.4 and were incubated for 24 h at 25 °C in an anaerobic environment before measuring circular dichroism (CD) at 216 and 231 nm using a J715 spectropolarimeter (Jasco Research Ltd.). Data were fit to a two-state monomer unfolding model as described (9) according to Eq. **S11**:

$$Y_{\mathrm{obs}} = \{(Y_N^o - S_N[\mathrm{urea}] - [(Y_N^o - S_N[\mathrm{urea}]) - (Y_U^o - S_u[\mathrm{urea}])]\} e^{\frac{m([\mathrm{urea}] - C_{\mathrm{mid}})}{\mathrm{RT}}} / 1 + e^{\frac{m([\mathrm{urea}] - C_{\mathrm{mid}})}{\mathrm{RT}}}, \quad \textbf{[S11]}$$

where, Y_{obs} is the observed optical signal, Y_N^o and Y_u^o are the native and unfolded signals, respectively, in the absence of urea, and S_N and S_U describe the dependence of the native and

unfolded signals with urea, respectively. m is a constant that describes the dependence of the free energy of unfolding (ΔG_u) on urea concentration and C_{mid} is the concentration of urea at the midpoint of the curve, corresponding to the point at which $f_u = 0.5$.

Acquiring Predicted Aggregation Propensities from a Variety of Known Algorithms. In order to further investigate aggregation mechanisms, the following methods were used to compare predicted mutant SOD1 aggregation with observed reduced apo mutant SOD1 aggregation and disease duration: Chiti et al. (10) and Wang et al. (11) methods, and online algorithms including Zyggregator (http://www-vendruscolo.ch.cam.ac.uk/zyggregator.php) (12), PASTA (http://protein.cribi.unipd.it/pasta/) (13), Waltz (http://waltz.switchlab.org/) (14), TANGO (http://tango.crg.es/) (15), FoldAmyloid (http://antares.protres.ru/fold-amyloid/oga.cgi) (16), and Profile3D (http://services.mbi.ucla.edu/zipperdb/) (17). Predictions were made for pseudo WT (pWT) and all 12 mutants presented in this study. Additionally, 13 extra mutants with disease duration averages based on 5 or more patients (11) were predicted and included in the correlations for disease duration. All results were compared to pWT and no convincing correlations between predicted aggregation propensity and observed aggregation or familial amyotrophic lateral sclerosis (fALS) disease duration were observed.

1. Sturtevant JM (1987) Biochemical applications of differential scanning calorimetry. *Annu Rev Phys Chem* 38:463–488.
2. Consalvi V, et al. (2000) Thermal unfolding and conformational stability of the recombinant domain II of glutamate dehydrogenase from the hyperthermophile Thermotoga maritima. *Protein Eng* 13:501–507.
3. Jha BK, et al. (2004) pH and cation-induced thermodynamic stability of human hyaluronan binding protein 1 regulates its hyaluronan affinity. *J Biol Chem* 279:23061–23072.
4. McCrary BS, Bedell J, Edmondson SP, Shriver JW (1998) Linkage of protonation and anion binding to the folding of Sac7d. *J Mol Biol* 276:203–224.
5. Yang ZW, et al. (2004) Dimethyl sulfoxide at 2.5% (v/v) alters the structural cooperativity and unfolding mechanism of dimeric bacterial NAD+ synthetase. *Protein Sci* 13:830–841.
6. Stathopulos PB, et al. (2006) Calorimetric analysis of thermodynamic stability and aggregation for apo and holo amyotrophic lateral sclerosis-associated Gly-93 mutants of superoxide dismutase. *J Biol Chem* 281:6184–6193.
7. Briere LK, Dunn SD (2006) The periplasmic domains of Escherichia coli HflKC oligomerize through right-handed coiled-coil interactions. *Biochemistry* 45:8607–8616.
8. Vassall KA, Stathopulos PB, Rumfeldt JA, Lepock JR, Meiering EM (2006) Equilibrium thermodynamic analysis of amyotrophic lateral sclerosis-associated mutant apo Cu,Zn superoxide dismutases. *Biochemistry* 45:7366–7379.
9. Pace CN (1986) Determination and analysis of urea and guanidine hydrochloride denaturation curves. *Methods Enzymol* 131:266–280.
10. Chiti F, Stefani M, Taddei N, Ramponi G, Dobson CM (2003) Rationalization of the effects of mutations on peptide and protein aggregation rates. *Nature* 424:805–808.
11. Wang Q, Johnson JL, Agar NY, Agar JN (2008) Protein aggregation and protein instability govern familial amyotrophic lateral sclerosis patient survival. *PLoS Biol* 6:e170.
12. Tartaglia GG, Vendruscolo M (2008) The Zyggregator method for predicting protein aggregation propensities. *Chem Soc Rev* 37:1395–1401.
13. Trovato A, Chiti F, Maritan A, Seno F (2006) Insight into the structure of amyloid fibrils from the analysis of globular proteins. *PLoS Comput Biol* 2:e170.
14. Maurer-Stroh S, et al. (2010) Exploring the sequence determinants of amyloid structure using position-specific scoring matrices. *Nat Methods* 7:237–242.
15. Fernandez-Escamilla AM, Rousseau F, Schymkowitz J, Serrano L (2004) Prediction of sequence-dependent and mutational effects on the aggregation of peptides and proteins. *Nat Biotechnol* 22:1302–1306.
16. Garbuzynskiy SO, Lobanov MY, Galzitskaya OV (2010) FoldAmyloid: A method of prediction of amyloidogenic regions from protein sequence. *Bioinformatics* 26:326–332.
17. Goldschmidt L, Teng PK, Riek R, Eisenberg D (2010) Identifying the amylome, proteins capable of forming amyloid-like fibrils. *Proc Natl Acad Sci USA* 107:3487–3492.

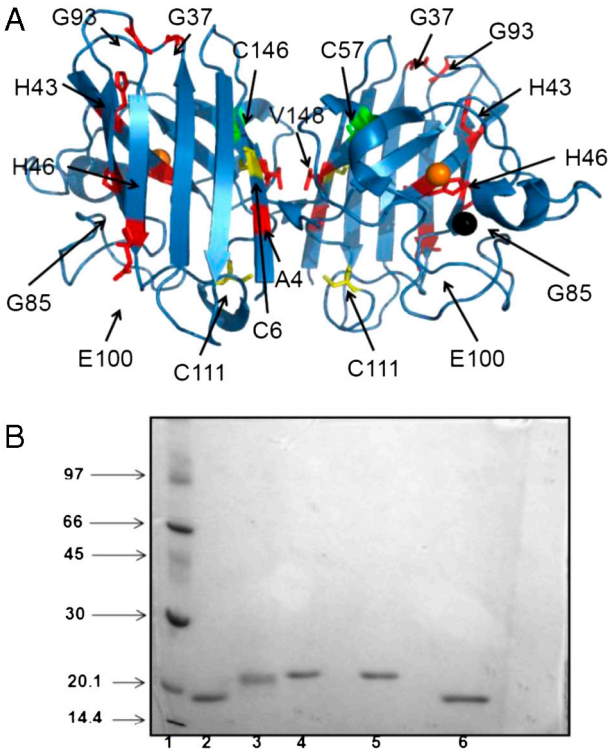

Fig. S1. (*A*) Ribbon representation of holo SOD1 (PDB ID code 1HL5) (1). Each monomer binds one zinc and one copper ion, indicated by black and gold spheres, respectively. The locations of C57 and C146, which form the intramolecular disulfide bond in each monomer, are shown in green. The sites of the fALS-associated mutations that were investigated in this study (A4, G37, H43, H46, G85, G93, E100G, and V148) are shown in red. The fALS mutations are dispersed throughout the structure of SOD1 and have a range of structural contexts. H46R and G85R (2, 3) alter metal binding, A4S, A4T, A4V, and V148 are located in the dimer interface, G93S, A, and R are in a tight turn, G37R and H43R disrupt packing in the β-barrel (4, 5), and E100G removes a salt bridge with K30 (6). Residues C6 and C111 are mutated to A and S, respectively, in the pWT construct and are shown in yellow. The figure was rendered using Pymol. (*B*) SDS-PAGE of reduced apo SOD1 before and after DSC experiments. The gel contained 12% acrylamide and was visualized by staining with Coomassie Blue. Lane 1 is a low molecular weight marker with molecular weights as indicated. Lanes 2 and 6 are disulfide-intact apo SOD1 controls, whereas lane 3 is apo SOD1 with disulfide reduced by β-mercaptoethanol. Lanes 4 and 5 are reduced apo SOD1 in 20 mM Hepes, 1 mM TCEP, pH 7.4 before and after DSC scanning, respectively. These samples were treated with iodoacetamide prior to loading on the gel to prevent free cysteines from being oxidized on the gel (7). Samples, both before and after each experiment, were found to run much closer to the disulfide-reduced control in lane 3 than the oxidized controls in lanes 2 and 6, indicating that the samples remained fully reduced throughout each experiment.

1. Strange RW, et al. (2003) The structure of holo and metal-deficient wild-type human Cu, Zn superoxide dismutase and its relevance to familial amyotrophic lateral sclerosis. *J Mol Biol* 328:877–891.
2. Antonyuk S, et al. (2005) Structural consequences of the familial amyotrophic lateral sclerosis SOD1 mutant His46Arg. *Protein Sci* 14:1201–1213.
3. Cao X, et al. (2008) Structures of the G85R variant of SOD1 in familial amyotrophic lateral sclerosis. *J Biol Chem* 283:16169–16177.
4. DiDonato M, et al. (2003) ALS mutants of human superoxide dismutase form fibrous aggregates via framework destabilization. *J Mol Biol* 332:601–615.
5. Hart PJ, et al. (1998) Subunit asymmetry in the three-dimensional structure of a human CuZnSOD mutant found in familial amyotrophic lateral sclerosis. *Protein Sci* 7:545–555.
6. Rumfeldt JA, Stathopulos PB, Chakrabarrty A, Lepock JR, Meiering EM (2006) Mechanism and thermodynamics of guanidinium chloride-induced denaturation of ALS-associated mutant Cu,Zn superoxide dismutases. *J Mol Biol* 355:106–123.
7. Furukawa Y, O'Halloran TV (2005) Amyotrophic lateral sclerosis mutations have the greatest destabilizing effect on the apo- and reduced form of SOD1, leading to unfolding and oxidative aggregation. *J Biol Chem* 280:17266–17274.

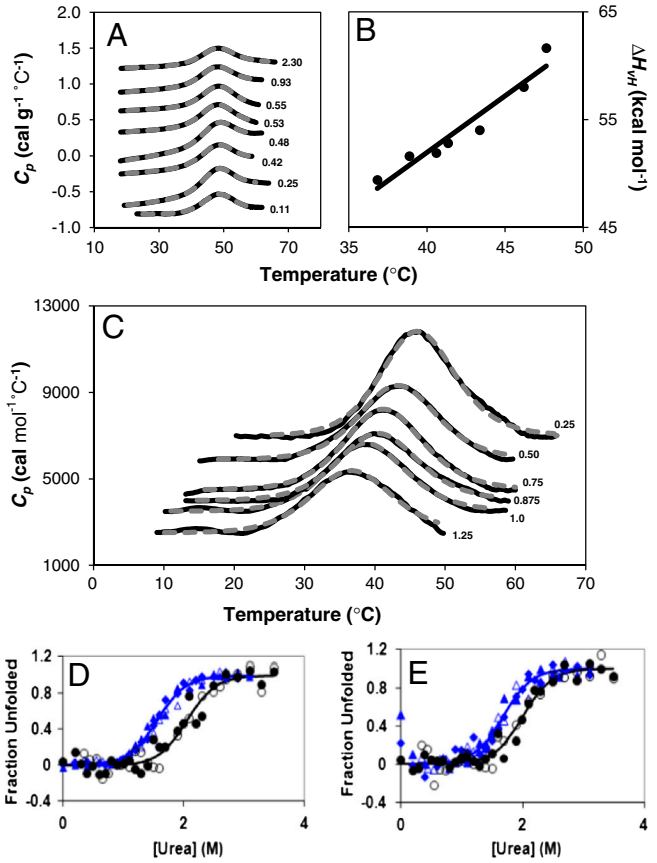

Fig. S2. (*A*) Protein concentration dependence of reduced apo pWT thermal unfolding. DSC endotherms were collected in 20 mM Hepes, 1 mM TCEP, pH 7.4 at different protein concentrations as indicated (in mg mL^{-1}). There is no concentration dependent shift to higher temperatures of unfolding, as expected for a monomer. The data (solid black lines) over the >20-fold concentration range are well fit (broken grey lines) by a monomer two-state unfolding model (*SI Materials and Methods*, Eq. **S1**). Fitted parameters are given in Table S1. (*B*) Kirchoff plot analysis of ΔC_p. The ΔH_{vH} values were obtained from two-state monomer fitting of pWT DSC data collected in the presence of urea (see *D* and *E*). The ΔH_{vH} data are well fit by linear regression ($r = 0.967$) giving a ΔC_p value from the slope of 1.1 ± 0.1 kcal mol^{-1} °C^{-1}. (*C*) Reduced apo pWT DSC scans in urea. Baselines generated by the linear connect method in Origin 5.0 (Microcal) were subtracted from raw data and normalized for protein concentration, prior to fitting data to a two-state monomer unfolding model (*SI Materials and Methods*, Eq. **S1**). Fits (broken grey lines) are shown for data (solid black lines) collected in 20 mM Hepes, 1 mM TCEP, pH 7.4 with 0.25, 0.5, 0.75, 0.875, 1, and 1.25 M urea (*Top* to *Bottom*) as indicated. ΔH_{vH} values from the fits are plotted in Fig. S2*A*. (*D* and *E*) Equilibrium urea renaturation and denaturation curves for reduced apo SOD1 at 25 °C. Data for pWT are shown in blue and data for H46R are shown in black. Protein concentrations for the curves are 8.5 μM (0.13 mg mL^{-1}) (circles), 14 μM (0.22 mg mL^{-1}) (triangles), and 24 μM (0.38 mg mL^{-1}) (diamonds). Denaturation and renaturation data are plotted as closed and open symbols, respectively. CD data for each protein at (*D*) 216 nm and (*E*) 231 nm were globally fit to a two-state monomer unfolding model with C_{mid} and *m* as shared parameters (*SI Materials and Methods*, Eq. **S11**). pWT and H46R yielded similar *m* values with the average being 2.49 ± 0.30 kcal mol^{-1}, whereas the midpoint of denaturation (C_{mid}) for pWT was 1.63 ± 0.07 M and 2.04 ± 0.04 M for H46R, corresponding to ΔG of 4.0 ± 0.2 kcal mol^{-1} and 5.1 ± 0.1 kcal mol^{-1} for pWT and H46R, respectively (Table 1).

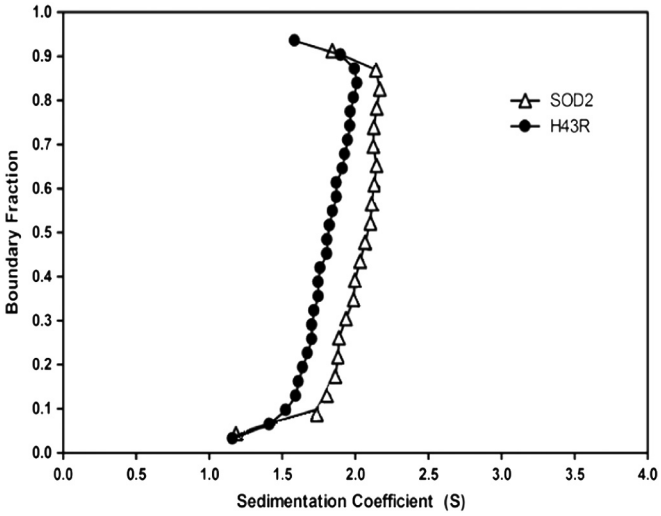

Fig. S3. Van Holde–Weischet analysis (1) of sedimentation velocity analytical ultracentrifugation experiments for reduced apo pWT and H43R SOD1. Experiments were conducted in 20 mM Hepes, 1 mM TCEP, pH 7.4 at 20 °C using an Optima XL-A Analytical Ultracentrifuge (Beckman Coulter Inc.) with an An60Ti rotor and two channel cells with Epon-charcoal centerpieces and absorbance detection at 280 nm. All velocity data were acquired at 50,000 rpm with measurements (average of three readings) collected at radial step sizes of 0.003 cm; scans were taken at 10-min intervals for a total of 30 scans. Data were analyzed using the program Sedfit (2). The initial absorbances at 280 nm were 0.29 and 0.33 for pWT and H43R, respectively.

1. van Holde KE, Weischet, WO (1978) Boundary analysis of sedimentation velocity experiments with monodisperse and paucidisperse solutes. *Biopolymers* 17:1387–1403.
2. Schuck P (2007) Sedimentation equilibrium analytical ultracentrifugation for multicomponent protein interactions. *Protein Interactions: Biophysical Approaches for the Study of Complex Reversible Systems*, ed Atassi MZ (Springer, New York), Vol 5, pp 289–316.

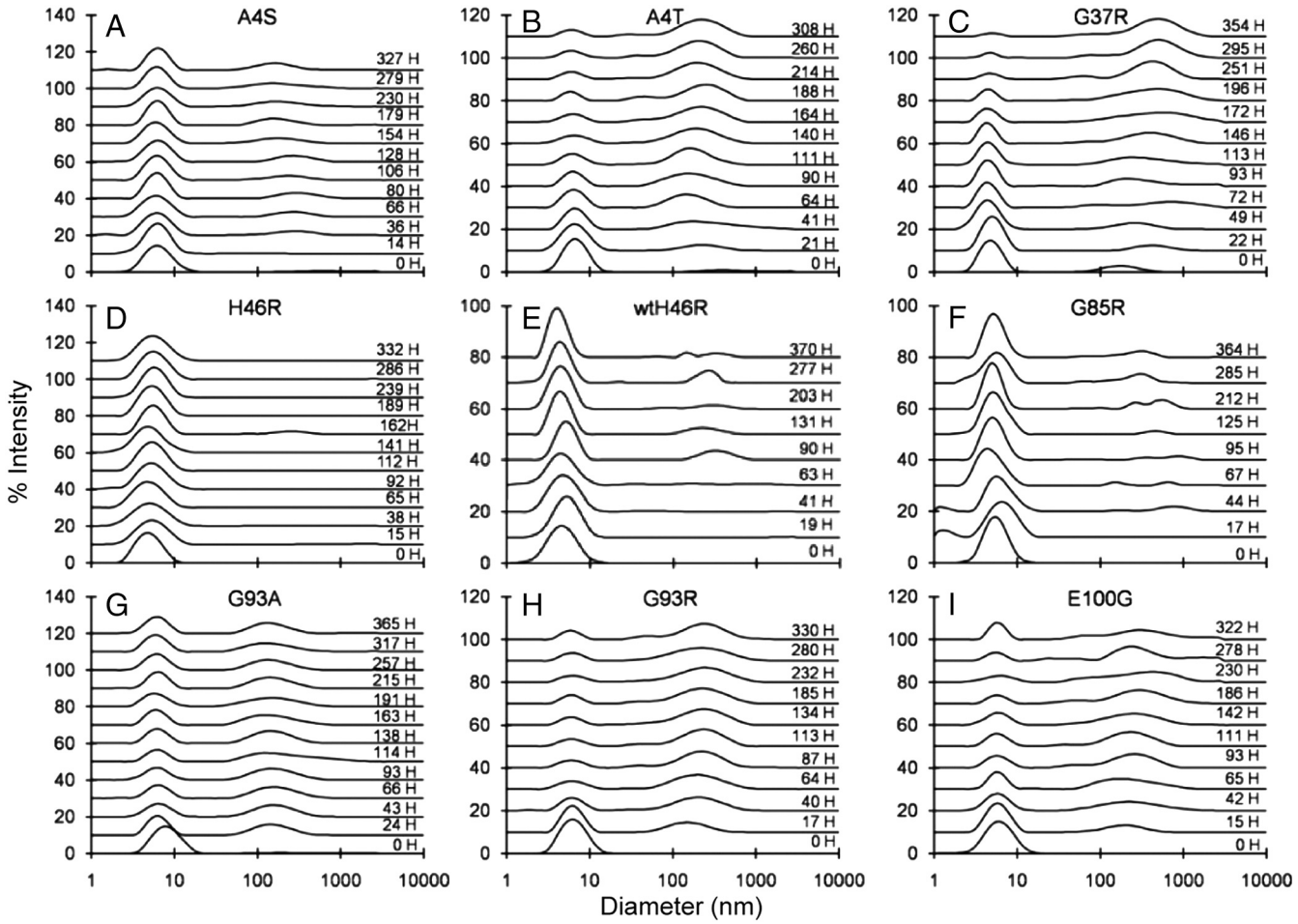

Fig. S4. Particle size distributions for reduced apo (*A*) A4S, (*B*) A4T, (*C*) G37R, (*D*) H46R, (*E*) wtH46R, (*F*) G85R, (*G*) G93A, (*H*) G93R, and (*I*) E100G as a function of incubation time in hours (H). Samples contained ~1 mg mL^{-1} protein in 20 mM Hepes, 1 mM TCEP, pH 7.4. The differing aggregation tendencies of each mutant are shown. The monomer remains the dominant species and after incubating G85R, H46R, and wtH46R for ~300 h, whereas diminished monomer intensity and varying amounts of larger species form after incubating A4S, A4T, G37R, G93A, G93R and E100G under the same conditions. There is no significant difference in the aggregation behavior of H46R in the pWT and WT background.

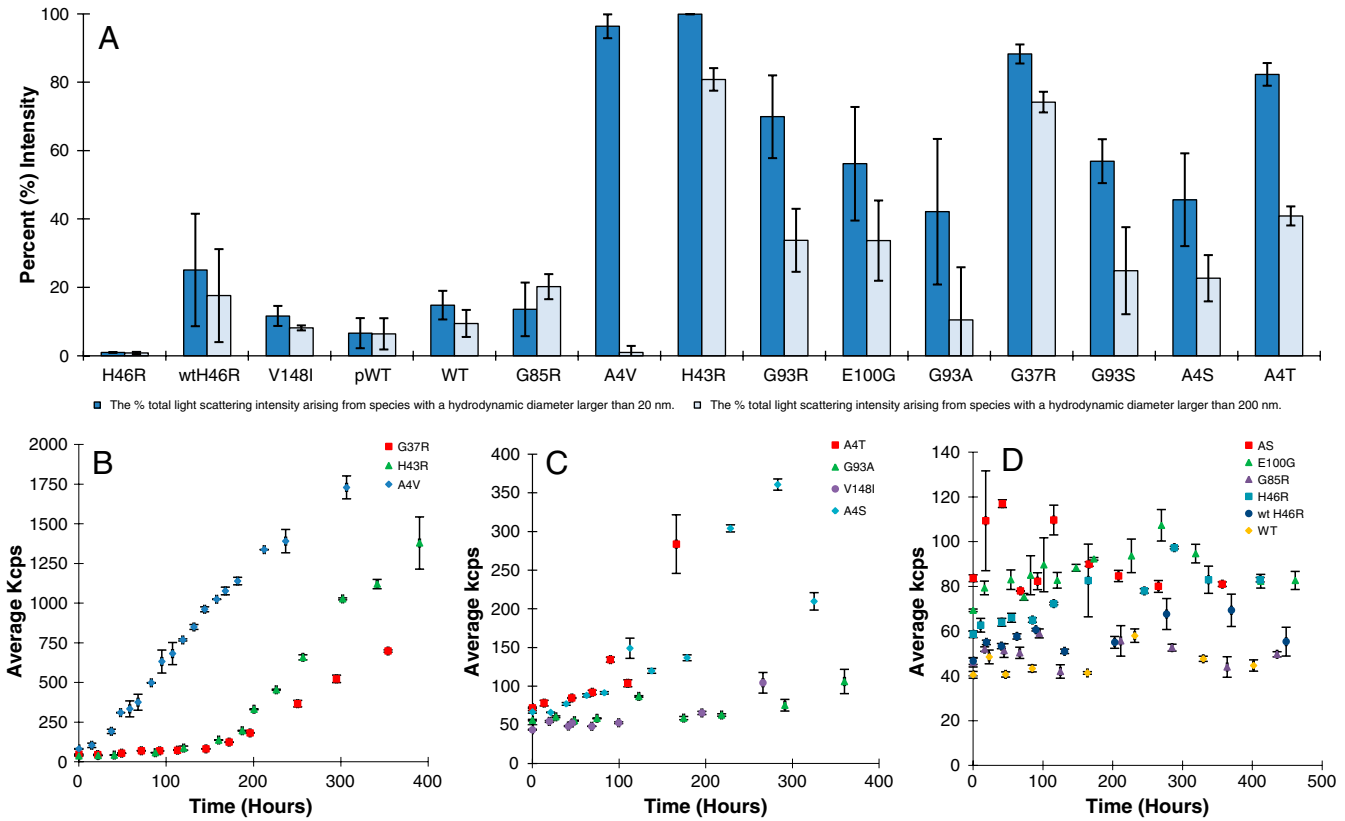

Fig. S5. (*A*) To address reproducibility, each DLS experiment was repeated between two and five times and the percent of total light scattering intensity after incubation for ~300 h arising from species with a hydrodynamic diameter larger than 20 nm (dark blue bars) and 200 nm (light blue bars) was compared. The reproducibility of each DLS experiment is reflected by the error bars. (*B–D*) Change in light scattering intensity [in kilocounts per second (kcps)] as a function of incubation time is shown for all mutants studied. All values plotted are an average of three measurements at each time point shown over the duration of the time course. The data acquired for each mutant were categorized into three plots: (*B*) mutants that showed significant aggregation, (*C*) mutants that show evidence for slight to moderate increased aggregation tendencies, and (*D*) mutants that showed very little to no evidence of aggregation.

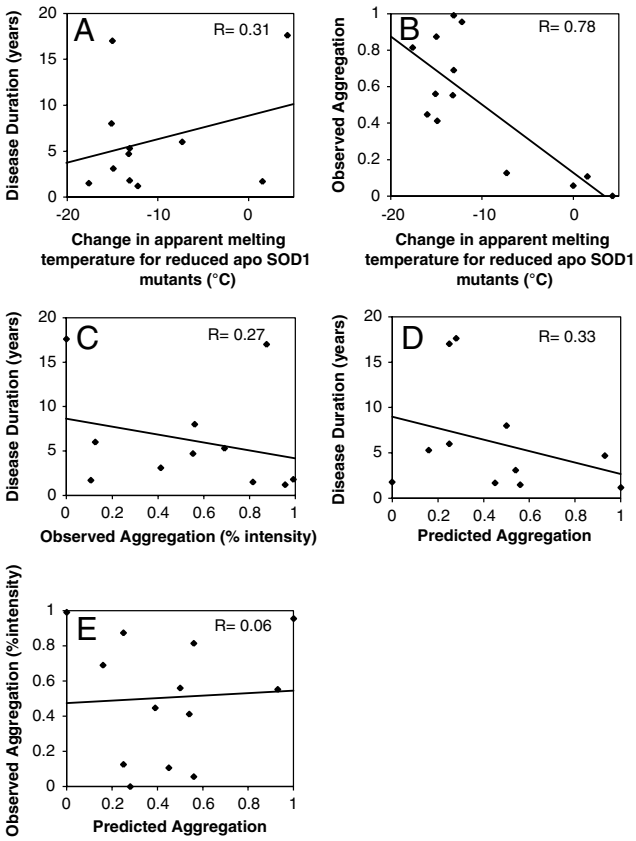

Fig. S6. A correlation plot of reduced apo SOD1 mutant stability, observed aggregation, predicted aggregation propensity and disease duration. Stability is represented as the change in $t_{m,app}$ for reduced apo SOD1 upon mutation. Observed aggregation values are based on light scattering intensity at the end of each mutant SOD1 DLS time course (see Fig. S5*A*). Predicted aggregation was assessed for SOD1 mutants based on the Chiti et al. method (10). Aggregation values are normalized in such a way that 1 represents the most aggregation and 0 represents the least aggregation. Finally, disease duration is based on summarized data by Wang et al. (11) and is normalized so that 1 represents mutants with the longest disease durations and 0 represents mutants with the shortest disease durations. (*A*) A poor correlation is observed between mutant reduced apo SOD1 stability and disease duration. (*B*) Increased observed reduced apo SOD1 aggregation correlates well with a decrease in mutant stability. Disease duration is poorly correlated with observed reduced apo SOD1 aggregation (*C*) and predicted SOD1 aggregation (*D*). (*E*) There is no correlation between observed and predicted aggregation. Refer to Table S2.

Table S1. DSC monomer two-state unfolding fitted parameters for disulfide-reduced apo superoxide dismutases (SOD1s)

apo reduced SOD1	[Protein], mg/mL	t_m,* °C	$\Delta C_p(t_m)$,† kcal(mol)$^{-1}$ °C^{-1}	$\Delta H_{vH}(t_m)$,‡ kcal(mol)$^{-1}$	$\Delta H_{cal}(t_m)$,‡ kcal(mol)$^{-1}$	$\Delta H_{vH}/\Delta H_{cal}$
pWT	0.11	47.3 ± 0.1	1.12	63.5 ± 1.7	47.9 ± 0.8	1.33
pWT	0.25	47.0 ± 0.5	1.66	60.4 ± 1.1	62.6 ± 0.7	0.96
pWT	0.42	47.4 ± 0.3	0.88	63.2 ± 2.8	52.4 ± 1.9	1.21
pWT	0.48	47.8 ± 0.6	0.80	62.5 ± 5.4	59.4 ± 4.0	1.05
pWT	0.53	47.5 ± 0.0	0.71	60.2 ± 0.6	60.2 ± 0.4	1.00
pWT	0.55	48.8 ± 0.0	−0.27	60.6 ± 0.7	59.8 ± 0.4	1.01
pWT	0.93	47.7 ± 0.3	0.27	62.7 ± 3.2	51.2 ± 1.9	1.22
pWT	2.30	47.5 ± 0.1	0.61	59.8 ± 1.7	44.6 ± 0.8	1.34
Avg ± SD§		47.6 ± 0.5	0.72 ± 0.57	61.6 ± 1.5	54.8 ± 6.6	1.14 ± 0.15
H46R	0.33	52.3 ± 0.1	−0.05	77.1 ± 2.1	75.6 ± 1.2	1.02
H46R	0.48	52.5 ± 0.0	0.17	70.5 ± 0.8	80.9 ± 0.1	0.87
H46R	0.57	53.2 ± 0.2	−1.39	70.5 ± 2.9	73.2 ± 1.6	0.96
Avg ± SD§		52.6 ± 0.5	−0.42 ± 0.84	72.7 ± 3.8	76.5 ± 4.0	0.95 ± 0.08
V148I	0.74	51.8 ± 0.9	−3.46	56.6 ± 9.4	58.4 ± 3.8	0.97
V148I	0.89	50.3 ± 0.1	−1.77	60.3 ± 1.3	67.0 ± 0.8	0.90
Avg ± SD§		51.0 ± 1.1	−2.62 ± 1.19	58.4 ± 2.6	62.7 ± 6.1	0.93 ± 0.05
G85R	0.17	40.6 ± 2.0	−0.46	52.2 ± 13.9	74.3 ± 13.2	0.70
G85R	0.38	40.4 ± 0.6	0.22	50.9 ± 3.8	47.1 ± 2.5	1.08
G85R	1.42	41.2 ± 0.2	−0.11	49.3 ± 1.5	35.0 ± 0.7	1.41
Avg ± SD§		40.7 ± 0.4	−0.11 ± 0.34	50.8 ± 1.5	52.3 ± 20.2	1.06 ± 0.36
E100G	0.43	35.0 ± 0.1	0.32	42.2 ± 1.0	32.8 ± 0.4	1.24
E100G	0.49	32.7 ± 1.1	0.87	45.5 ± 6.8	37.9 ± 4.8	1.20
E100G	0.75	33.0 ± 0.1	0.89	43.4 ± 1.3	32.3 ± 0.7	1.34
E100G	0.80	32.1 ± 0.1	1.07	42.1 ± 1.2	32.6 ± 0.5	1.29
Avg ± SD§		33.2 ± 1.2	0.79 ± 0.32	43.3 ± 1.4	34.3 ± 2.6	1.27 ± 0.06
WT	0.34	46.5 ± 0.0	0.53	57.9 ± 1.0	34.7 ± 0.25	1.68
WT	0.30	47.1 ± 0.7	1.48	56.4 ± 7.4	43.3 ± 3.75	1.30
Avg ± SD§		46.8 ± 0.4	1.01 ± 0.67	57.2 ± 1.1	39.0 ± 6.1	1.49 ± 0.27
WT H46R	0.50	50.4 ± 0.0	−1.86	55.5 ± 0.9	64.9 ± 0.63	0.86
WT H46R	0.50	52.5 ± 0.2	−0.40	63.6 ± 1.6	70.9 ± 1.26	0.90
WT H46R	0.50	52.6 ± 0.6	−0.77	64.4 ± 6.0	85.2 ± 5.19	0.76
Avg ± SD§		51.8 ± 1.3	−1.01 ± 0.76	61.2 ± 4.9	73.7 ± 10.4	0.84 ± 0.07

*Errors (±) from the fitting program (Microcal Origin, version 5.0).
†Errors from individual fits could not be reliably determined because they are based on uncertainties in five independent variables.
‡Errors derived using standard procedures (1) from errors in fitted $\Delta h_{cal}(t_m)$ and β returned by the fitting program.
§Average and standard deviation.

1. Taylor JR (1982) *An Introduction to Error Analysis* (University Science Books, Mill Valley, CA).

Table S2. Stability and aggregation summary for disulfide-reduced apo SOD1s

apo SOD1	t_m (disulfide-reduced),* °C	Δt_m (disulfide-reduced),† °C	Δt_m (disulfide-oxidized),†,‡ °C	Disease duration, y§	Predicted aggregation propensity¶	Predicted aggregation propensity + instability‖	Observed aggregation propensity**
H46R	52.8 ± 0.4	+4.3	+3.0	17.6	0.28	0.00	0.00
V148I	50.0 ± 0.1	+1.5	+1.4	1.7	0.45	0.20	0.11
pWT	48.5 ± 0.3	NA	NA	NA	0.56	0.32	0.06
G85R	41.2 ± 0.3	−7.3	−3.8	6.0	0.25	0.34	0.13
A4V	36.3 ± 0.2	−12.2	−8.9	1.2	1.00	1.0	0.96
H43R	35.4 ± 0.4	−13.1	−10.7	1.8	0.00	0.35	1.00
G93R	35.4 ± 1.8	−13.1	−10.1	5.3	0.16	0.46	0.70
E100G	35.3 ± 0.7	−13.2	−7.7	4.7	0.93	0.98	0.56
G93A	34.6††	−14.9	−10.3	3.1	0.54	0.77	0.42
G37R	33.5 ± 1.2	−15.0	−9.7	17	0.25	0.58	0.88
G93S	33.4 ± 1.2	−15.1	−8.6	8.0	0.50	0.75	0.53
A4S	32.5††	−16.0	−13.0	NA	0.39	0.70	0.45
A4T	30.9 ± 0.3	−17.6	−14.9	1.5	0.56	0.87	0.82

NA, not applicable.

*Values are the apparent melting temperature where the observed C_p in the DSC scan is a maximum. The values listed are the average of at least two independent measurements unless otherwise noted.

†Calculated as $t_{m,\text{app mutant}} - t_{m,\text{app WT}}$, negative values indicate destabilization.

‡$\Delta t_{m,\text{app}}$ data for A4V, G85R, E100G, G93S, and G93R were obtained from (6, 8). The $\Delta t_{m,\text{app}}$ for H46R, V148I, H43R, G93A, G37R, A4S, and A4T was obtained from scans acquired in this study.

§Average disease durations are from Wang et al. (11).

¶Predicted aggregation propensities were calculated relative to pWT using the Chiti-Dobson method (10) and normalized using the methodology of Wang et al. (11), where 0 indicates low aggregation propensity and 1 indicates high aggregation tendency.

‖$\Delta t_{m,\text{app}}$ incorporated into the predicted aggregation propensity as described by Wang et al. (11), and aggregation scores were normalized over a scale from 0 to 1.

**Observed aggregation propensity is based on intensity statistics from DLS measurements as shown in Fig. S5*A*.

††$t_{m,\text{app}}$ based on one measurement.

Table S3. Single species model fitting of analytical ultracentrifugation sedimentation equilibrium data

Sample and concentrations		Best fit molecular weight (kDa) ± standard error at different rotor speeds			
Apo reduced SOD	[SOD], mg/mL	20,000 rpm	25,000 rpm	30,000 rpm	35,000 rpm
pWT	1.0	15.2 ± 0.4	15.0 ± 0.2	14.3 ± 0.2	13.5 ± 0.2
pWT	1.0	14.3 ± 0.3	15.1 ± 0.3	15.2 ± 0.2	14.1 ± 0.1
pWT	1.5	14.4 ± 0.3	15.6 ± 0.2	14.4 ± 0.1	12.4 ± 0.1
E100G	0.8	22.5 ± 0.4	21.3 ± 0.2	19.3 ± 0.2	17.5 ± 0.1
E100G	1.0	20.3 ± 0.4	19.3 ± 0.3	17.4 ± 0.2	16.6 ± 0.2
E100G	1.5	20.2 ± 0.3	19.3 ± 0.2	17.8 ± 0.2	16.4 ± 0.1
A4V	0.8	24.2 ± 0.6	21.1 ± 0.3	18.2 ± 0.2	16.5 ± 0.1
H43R	1.0	36.6 ± 0.6	31.6 ± 0.6	23.2 ± 0.3	19.8 ± 0.2
H43R	1.0	33.6 ± 0.4	28.4 ± 0.3	23.2 ± 0.2	20.5 ± 0.1